European Journal of Pharmaceutics and Biopharmaceutics 80 (2012) 535–543

Contents lists available at SciVerse ScienceDirect

European Journal of Pharmaceutics and Biopharmaceutics

journal homepage: www.elsevier.com/locate/ejpb

Research paper

Uniform mesoporous carbon as a carrier for poorly water soluble drug and its cytotoxicity study

Peng Zhao [a], Lihong Wang [b], Changshan Sun [a], Tongying Jiang [a], Jinghai Zhang [c], Qiang Zhang [d], Jin Sun [a], Yihui Deng [a], Siling Wang [a,*]

[a] Department of Pharmaceutics, Shenyang Pharmaceutical University, Shenyang, China
[b] Department of Pharmaceutical Engineering, Shenyang Pharmaceutical University, Shenyang, China
[c] Department of Life Science and Biopharmaceutics, Shenyang Pharmaceutical University, Shenyang, China
[d] Department of Pharmaceutics, Peking University, Beijing, China

ARTICLE INFO

Article history:
Received 6 August 2011
Accepted in revised form 5 December 2011
Available online 13 December 2011

Keywords:
Drug delivery system
Mesoporous carbon
Poorly water soluble drug
Increased dissolution rate
Cytotoxicity

ABSTRACT

In this study, uniform mesoporous carbon spheres (UMCS) with 3-D pore system and fibrous ordered mesoporous carbon (FOMC) with 2-dimensional hexagonal mesoporous structure were studied as drug carriers for oral drug delivery system. Lovastatin (LOV), which has low water solubility, was chosen as a model drug. Drug release rate and degree of drug loading of UMCS and FOMC were compared. The effects of different pore channel structures and pore sizes on LOV uptake and release were systematically investigated. Cytotoxicity of UMCS and FOMC on human colon carcinoma (Caco-2) cells were also studied. The results indicate that UMCS has a higher degree of drug loading (up to 36.26% drug weight/total weight) compared with FOMC. The dissolution rate of LOV from UMCS was found to be markedly increased compared with pure crystalline LOV, and the dissolution rate of LOV from FOMC was relatively sustained compared with UMCS, and both UMCS and FOMC exhibited a weak cytotoxicity at tested concentrations (10–800 μg/ml).

1. Introduction

The oral route is the simplest method for administration. However, 40% of commercially available drugs or drugs under development are poorly water soluble [1], resulting in poor dissolution in gastrointestinal fluid and low oral bioavailability. Developing new and effective drug delivery systems to overcome this obstacle and to enhance therapeutic effects is a great challenge for scientists who are involved in pharmaceutical research and the search for new drug delivery vehicles.

Recently, porous materials (silica, carbon, oxides, etc.) have attracted great attention because of their special features [2–20]. There is no doubt that porous carbon possesses many advantages among these porous materials due to its inert nature, low toxicity, large surface area, pore volume, stronger adsorbability, and other physicochemical properties. To date, porous carbon has been used as an adsorbent, and in catalytic, electrochemical, separation, fuel, gas storage, and transport applications [21–31]. Mesoporous carbon with different shapes (nanotubes, polyhedrons, films, spheres, and fibers) can be synthesized by different methods and routes (hard-template method, soft-template method, and self-assembly method) [32–37]. However, there are few reports describing the use of porous carbon in drug delivery systems [38–40] and studies of an improvement in the dissolution rate and oral bioavailability of poorly water soluble drugs using uniform mesoporous carbon as a carrier. Mesoporous carbon has a higher surface area, larger pore volume, and stronger adsorbability than other porous materials, and, so, it is capable of a higher degree of drug loading. Moreover, carbon materials are inert substances that are safe and nontoxic. All of these features are advantages and support the potential benefit of using mesoporous carbon as a drug delivery vehicle.

In this study, Lovastatin was selected as model drug because of its poor water solubility and low oral bioavailability. UMCS with a 3-D pore system, different pore diameters (3.8–6.0 nm), and a high surface area (1069–1457 m^2/g) were synthesized at first time. The pharmaceutical performance of UMCS has not been studied, and this work is the first study of its application in a drug system involving loading with water insoluble drug for controlled release. The effects of different surface areas and pore diameters on the degree of drug loading and the release profile were

Abbreviations: UMCS, uniform mesoporous carbon spheres; FOMC, fibrous ordered mesoporous carbon; LOV, Lovastatin; Caco-2, human colon carcinoma; LOV–UMCS, drug-loaded samples using UMCS as carrier; LOV–FOMC, drug-loaded samples using FOMC as carrier.

* Corresponding author. Department of Pharmaceutics, Shenyang Pharmaceutical University, P.O. Box 23, 103 Wenhua Road, Shenhe District, Shenyang, Liaoning 110016, China. Tel./fax: +86 024 23986348.
E-mail address: silingwang@syphu.edu.cn (S. Wang).

0939-6411/$ - see front matter © 2011 Elsevier B.V. All rights reserved.
doi:10.1016/j.ejpb.2011.12.002

studied. Furthermore, FOMC with a 2-dimensional hexagonal mesoporous structure was synthesized, and studies were carried out to examine the effects of different morphologies and pore channel structures of mesoporous carbon on drug loading and controlled release. Cytotoxicity of carriers on Caco-2 cells was also investigated. Wide-angle X-ray scattering (WAXS), transmission electron microscopy (TEM), scanning electron microscopy (SEM), X-ray photoelectron spectroscopy (XPS), differential scanning calorimetry (DSC), surface area instrument, and cytotoxicity assays were used in this study. Cytotoxicity assays confirmed the safety of UMCS and FOMC, demonstrating the potential and advantages of mesoporous carbon as drug delivery vehicle. We believe this report will provide information to improve the dissolution rate and oral bioavailability of poorly water soluble drugs and, furthermore, improve their therapeutics effects while reducing their side effects.

2. Materials and methods

2.1. Materials

Hexadecylamine was purchased from Best-reagent Company (Chengdu, China). Pluronic 123 triblock polymer (P123) was obtained from Sigma–Aldrich (St. Louis, MO, USA). Fetal bovine serum was purchased from Tian Hang Biotechnology Co., Ltd. Caco-2 cells were purchased from Jia He Biotechnology Co., Ltd. (Shanghai, China). MTT was purchased from Amreso (USA). Tetraethyl orthosilicate (TEOS), isopropanol, hydrochloric acid, sulfuric acid, ammonia sucrose, DMSO, ethanol, formaldehyde, and hydrofluoric acid were purchased from Yu Wang Chemical Reagent Corporation (Shandong, China). Deionized water was obtained by ion exchange and used in all procedures.

2.2. Synthesis of uniform mesoporous carbon

2.2.1. Synthesis of UMCS

For this, 3–5 g hexadecylamine was added to a mixed solution containing 175 ml isopropanol and 225 ml deionized water under continuous stirring. Then, 15 ml tetraethoxysilane (TEOS) and 3.0–4.0 ml ammonia were added. Subsequently, the mixture was homogenized using a nanohomogenizer (AH100D, ATS Engineering Inc.), maintained at 25 °C for 18 h, and then purified by centrifugation. The precipitate was dried at 60 °C and then washed several times with ethanol and deionized water. Finally, mesoporous silica spheres (MSS) were obtained by calcination at 580 °C for 5.5 h. By adding different amount of hexadecylamine, MSS-1, MSS-2, and MSS-3 with different surface areas and pore volumes were obtained. Then, 1 g of MSS-1, MSS-2, and MSS-3 was added to a solution containing 0.5–0.8 g sucrose, 4 g H_2O, and 0.1 ml H_2SO_4, respectively. The mixtures were placed in a drying oven, maintained at 92 °C for 8 h, and then the temperature was increased to 160 °C for another 8 h. This was followed by the addition of 0.3–0.5 g sucrose, 0.09 ml H_2SO_4, and 4 g H_2O, and the mixtures were again subjected to the same process. Then, the samples were calcined at 800 °C for 6 h under N_2, and carbon–silica compounds (C–Si) were obtained. Finally, these C–Si samples were placed in 15% hydrofluoric acid for 24 h to remove silica, and UMCS samples were obtained.

UMCS-1 was synthesized using MSS-1 as a template, UMCS-2 was prepared using MSS-2 as a template, and UMCS-3 was obtained using MSS-3 as a template.

2.2.2. Synthesis of FOMC

SBA-15 was produced using a standard method with some modifications [41]; 1 g SBA-15 was added in a solution that contained 0.10 ml H_2SO_4, 5 ml H_2O, and 1.00–1.20 g sucrose at the first infiltration. The obtained mixture was placed in an oven at 80 °C for 8 h, and then the temperature was raised to 150 °C for another 8 h. At the second infiltration, the obtained sample was added in a solution containing 0.07 ml H_2SO_4, 5 ml H_2O, and 0.60–0.80 g sucrose and subjected to the same treatment described above. Then, the obtained mixture was carbonized at 700–800 °C under nitrogen gas. Finally, the silica template was removed by placing the sample in 15% hydrofluoric acid at 25 °C. FOMC samples (FOMC-1, FOMC-2, FOMC-3) with different pore diameters and surface areas were obtained by controlling the amount of sucrose and the calcination temperature.

2.3. Drug loading procedure

LOV belonging to Biopharmaceutical Classification System (BCS) II was selected as a model drug because of its poorly water solubility. The drug loading procedure was simple, and UMCS was added in a chloroform solution of LOV (60 mg/ml). Subsequently, the mixture solution was stirred for 14 h at 25 °C in a closed container. Finally, the precipitate was filtered and dried at 40 °C, and the obtained solid mixture (drug-loaded samples) was named LOV–UMCS. LOV–FOMC was prepared by the same drug loading process.

2.4. Characterization techniques

An SEM instrument (ZEISS, SUPRA 35, Germany) was used to investigate the morphology of the samples. The nanostructures of the samples were studied with a TEM apparatus (FEI, Tecnai G2 F20, the Netherlands).

The nitrogen adsorption isotherms and nanostructures of the samples were examined using a surface area instrument (Beckman Coulter, SA3100, USA). To remove adsorbed water, carriers were degassed at 120 °C for 10 h and drug-loaded samples were degassed at 60 °C for 10 h before analysis. The surface areas were calculated using the BET method, the pore diameter distributions were analyzed using the Barett–Joyner–Halenda (BJH) model, and the total pore volumes were determined using the amount adsorbed.

The WAXS patterns of the samples were recorded on an instrument (X'pert PRO, PANalytical B.V, the Netherlands), under operating conditions of 30 mA and 30 kV. The determination angle ranged from 5° to 50°, and the scan rate was 7°/min. The XPS spectra and composition of the surface layer of the samples were obtained using a spectrometer (Thermo VG, ESCALAB250, USA).

The DSC profiles of the samples were analyzed using a DSC instrument (TA Instruments, Q1000, USA). Drug-loaded samples equivalent to 1 mg LOV and 1 mg pure crystalline LOV were placed in aluminum pans and investigated. The temperature range was 50–200 °C at a heating rate of 10 °C/min.

2.5. Degree of drug loading

LOV was determined by HPLC (Hitachi, L2130 instrument, Japan). The chromatographic conditions used in the analysis were as follows: a C_{18} column (250 × 4.6 mm, 5 μm), a mobile phase of methanol/water (80:20), a UV detector of 238 nm, a flow rate of 1.0 ml/min, a column temperature of 35 °C, and an injection volume of 20 μl. LOV in drug-loaded samples was extracted with methanol under ultrasonic, then passed through a 0.22 μm filter, and analyzed by HPLC. Every sample was analyzed three times, and the mean value was used to calculate the drug loading. The degree of drug loading was calculated according to Eq. (1).

$$\text{Degree of drug loading } (\%) = \frac{\text{Weight of LOV in samples}}{\text{Weight of samples}} \times 100 \quad (1)$$

2.6. In vitro release profile testing

The dissolution profiles of pure crystalline LOV, and LOV from drug-loaded samples were determined using a dissolution instrument (Tianjin University Radio Factory, D 800 LS, China) according to the USP II paddle method. Enzyme-free buffer with 0.10% SDS (pH 6.8) was chosen as the dissolution medium; 20 mg of pure crystalline LOV and drug-loaded samples (equivalent to 20 mg LOV) was added to 900 ml dissolution medium and stirred at 50 rpm at 37 ± 0.5 °C for 90 min. Then, 5 ml samples of dissolution medium were withdrawn at specified times (5, 10, 15, 20, 30, 45, 60, and 90 min) and replaced with 5 ml fresh dissolution medium to maintain a constant volume. Then, the obtained samples were filtered, suitably diluted, and subjected to ultraviolet spectrophotometry (UV-2000, Unico, USA) at 238 nm. This procedure was carried out six times, and the mean value was used to calculate the dissolution rate of LOV from the samples.

2.7. Cytotoxicity assays

Caco-2 cells were chosen for in vitro cytotoxicity testing of UMCS and FOMC. Caco-2 cells were cultured in Dulbecco's modified Eagle's medium (DMEM, high glucose, 10% fetal bovine serum, L-glutamine, pyruvate, and nonessential amino acids) in culture flasks and incubated at 37 °C in an atmosphere of 5% CO_2, and the medium was changed every 2 days. In each test, the cell suspension was diluted with DMEM and seeded into 96-well plates at 100 μl per well and incubated for 24 h. Then, carrier suspensions containing different concentrations were added to 96-well plates at 20 μl per well and incubated for 24 h. Following this, 5 mg/ml MTT (thiazolyl blue tetrazolium bromide) solution was added to 96-well plates at 10 μl per well and incubated for 24 h. The solution was then removed and replaced with 100 μl DMSO. Finally, the absorbance was determined at 492 nm ($n = 6$), and the cell survival was calculated according to Eq. (2). An optical microscope (Olympus, IX 51, Japan) was used to examine the morphology of the Caco-2 cells.

$$\text{Cell Survival } (\%) = \frac{\text{Absorbance of sample}}{\text{Absorbance of control}} \times 100 \quad (2)$$

3. Results and discussion

3.1. Preparation of UMCS and FOMC

In the present experiment, both UMCS and FOMC were prepared using the hard-template method [38,39]. The major advantage of this method is that the pore structure could be ordered and the pore size can be easily controlled. For UMCS, its template (MSS) is spherical particles and it has a 3-D pore system. During the synthetic procedure, the pore walls of MSS were transformed into pore channels of UMCS and, so, UMCS also has a 3-D pore system. In addition, by controlling the adding amount of hexadecylamine, we can obtain MSS (MSS-1, MSS-2, MSS-3) with different thickness of pore walls, so we can control the pore size of UMCS by using different template. For FOMC, its template (SBA-15) possesses a fibrous morphology and a 2-dimensional hexagonal mesoporous structure; in the synthesis procedure, the pore walls of SBA-15 were transformed into the pore channels of FOMC, so FOMC also possesses 2-dimensional hexagonal mesoporous structure. In addition, by controlling the added amount of carbon source (sucrose) and the carbonization temperature, we obtained FOMC (FOMC-1, FOMC-2, FOMC-3) with different pore characteristics. The surface area and pore volume of FOMC-2 are lower than those of FOMC-1, and this may be due to the lower amount of sucrose added when preparing FOMC-2. This could result in the collapse of the carbon frame during the carbonization process and, so, the pore size of FOMC-2 was also slightly smaller compared with FOMC-1. For FOMC-3, its pore size was greater than that of FOMC-1, and this may be due to its lower carbonization temperature which may reduce the collapse of the carbon frame during the carbonization process.

3.2. SEM and TEM images

SEM and TEM were employed to characterize the morphology and nanostructures of UMCS, FOMC, and drug-loaded samples. As indicated in Fig. 1, UMCS is spherical and uniform with a particle size of about 500–800 nm. For UMCS, its surface was not smooth because of the presence of pore channels that are suitable for drug loading. As shown in Fig. 2, pure crystalline LOV is present and FOMC exhibits a fibrous morphology including aggregated rod-like sub-particles. To further examine the nanostructures of the samples, the TEM images of carriers and drug-loaded samples are shown in Figs. 3 and 4. The 3-D continuous pore channels of UMCS can be easily seen, and FOMC exhibits a 2-dimensional hexagonal mesoporous structure, arranged in an ordered array. Drugs can be absorbed and encapsulated in the pore channels during the drug loading procedure. They are then released from the pore channels during the absorption process. These pore channels also ensure

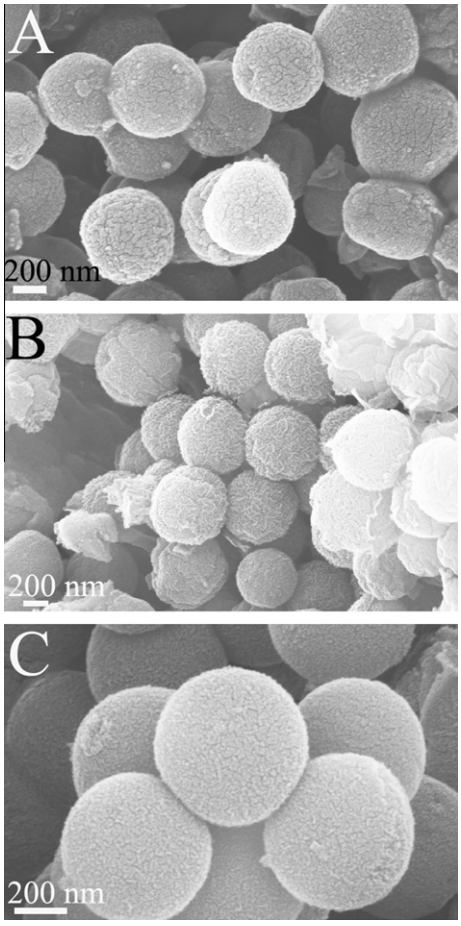

Fig. 1. SEM images of (A) UMCS-1, (B) UMCS-2, and (C) UMCS-3.

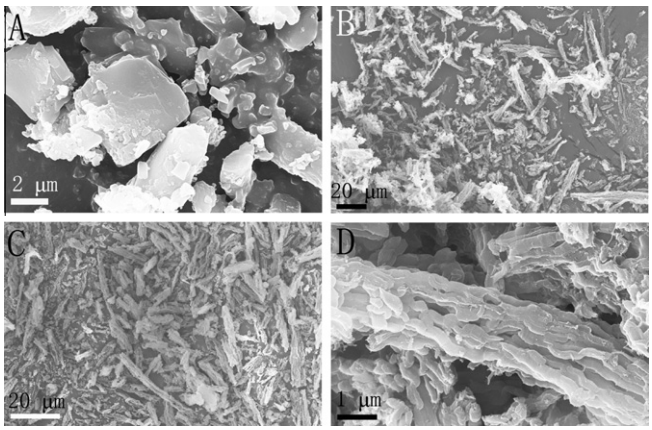

Fig. 2. SEM images of (A) pure crystalline LOV, (B) FOMC-1, (C) FOMC-2, and (D) FOMC-3.

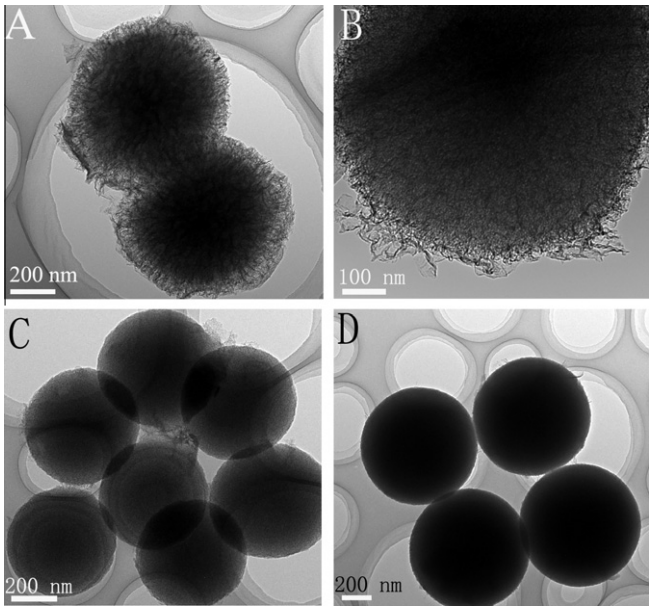

Fig. 3. TEM images of (A) UMCS-1, (B) UMCS-2, (C) UMCS-3, and (D) LOV–UMCS-1.

that the drugs are highly dispersed in the carriers and the drugs are prevented from aggregating; this also allows the drug to exist in the noncrystalline state, thereby improving the dissolution rate and absorption of the drugs in the gastrointestinal tract. In the case of the drug-loaded samples (Figs. 3D and 4D), their structures cannot be clearly seen and both LOV–UMCS and LOV–FOMC had a solid structure, indicating that most of the pore channels were filled with LOV in drug loading procedure.

3.3. Nanostructures and degree of drug loading

As seen in Fig. 5, typical type IV isotherms that have clear hysteresis loops were seen in all adsorption/desorption isotherms of UMCS and FOMC, indicating a mesoporous structure. The details of the nanoparticle characterization and degree of drug loading are shown in Table 1. The degree of drug loading for LOV–UMCS was high, which may attributed to its large pore volume, high surface area, and strong adsorbability. In the case of UMCS, the higher its pore volume and surface area are, the higher its degree of drug loading is. This was also confirmed by the degree of drug loading

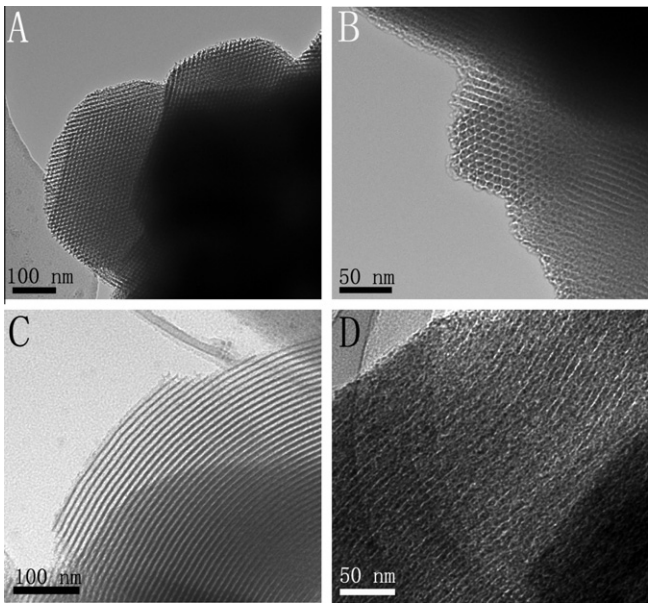

Fig. 4. TEM images of (A) FOMC-1, (B) FOMC-2, (C) FOMC-3, and (D) LOV–FOMC-1.

for LOV–FOMC which is relatively high. Mesoporous carbon possesses a low specific gravity of 12 g per mole, so it usually has a much higher surface area and pore volume than other mesoporous materials. It is also well known that carbon possesses a stronger adsorbability than most of other materials. All of these factors contribute to a high drug loading capacity, which illustrates many potential applications and advantages of using mesoporous carbon in drug delivery systems. The pore diameter distribution of UMCS and FOMC was uniform and ranged from 3 nm to 7 nm which is typical of mesopores. For the drug-loaded samples LOV–UMCS and LOV–FOMC, the shapes of the hysteresis loops in their adsorption/desorption isotherms were similar to those of UMCS and FOMC, indicating that the pore channel had not changed dramatically. However, the pore volume and surface area of the drug-loaded samples were reduced significantly, confirming that most pore channels of the carriers were filled with LOV.

3.4. WAXS studies

The WAXS patterns of pure crystalline LOV, UMCS, FOMC, the physical mixture, and drug-loaded samples with a determination angle ranging from 5° to 50° were studied (Fig. 6). Pure crystalline LOV that had a crystalline form exhibited numerous characteristic peaks in its diffraction pattern. For both physical mixtures (Fig. 6B and E), characteristic peaks of LOV were also clearly seen, which suggests that the crystalline form of LOV remained unchanged and there was no interaction between the pure drug and the carriers. However, hardly any characteristic peaks were observed in the drug-loaded samples LOV–UMCS and LOV–FOMC (Fig. 6C and F), suggesting that most of LOV loaded into UMCS and FOMC was in a noncrystalline state. This may be due to the smaller pore channels of UMCS and FOMC since, as we know, sufficient space is needed for the compounds to form an ordered structure and exist in the crystalline state. However, the pore size of UMCS and FOMC is only between 3 and 7 nm, which is not large enough for compounds to form a crystalline state, and, so, most of the drugs loaded into carriers were in a noncrystalline state. This was also proved by DSC analysis. In addition, the particle size of LOV in the drug-loaded samples is much smaller than that of crude LOV, so the surface area of drug increased significantly, which is a main reason for the increase in dissolution. Moreover, for most

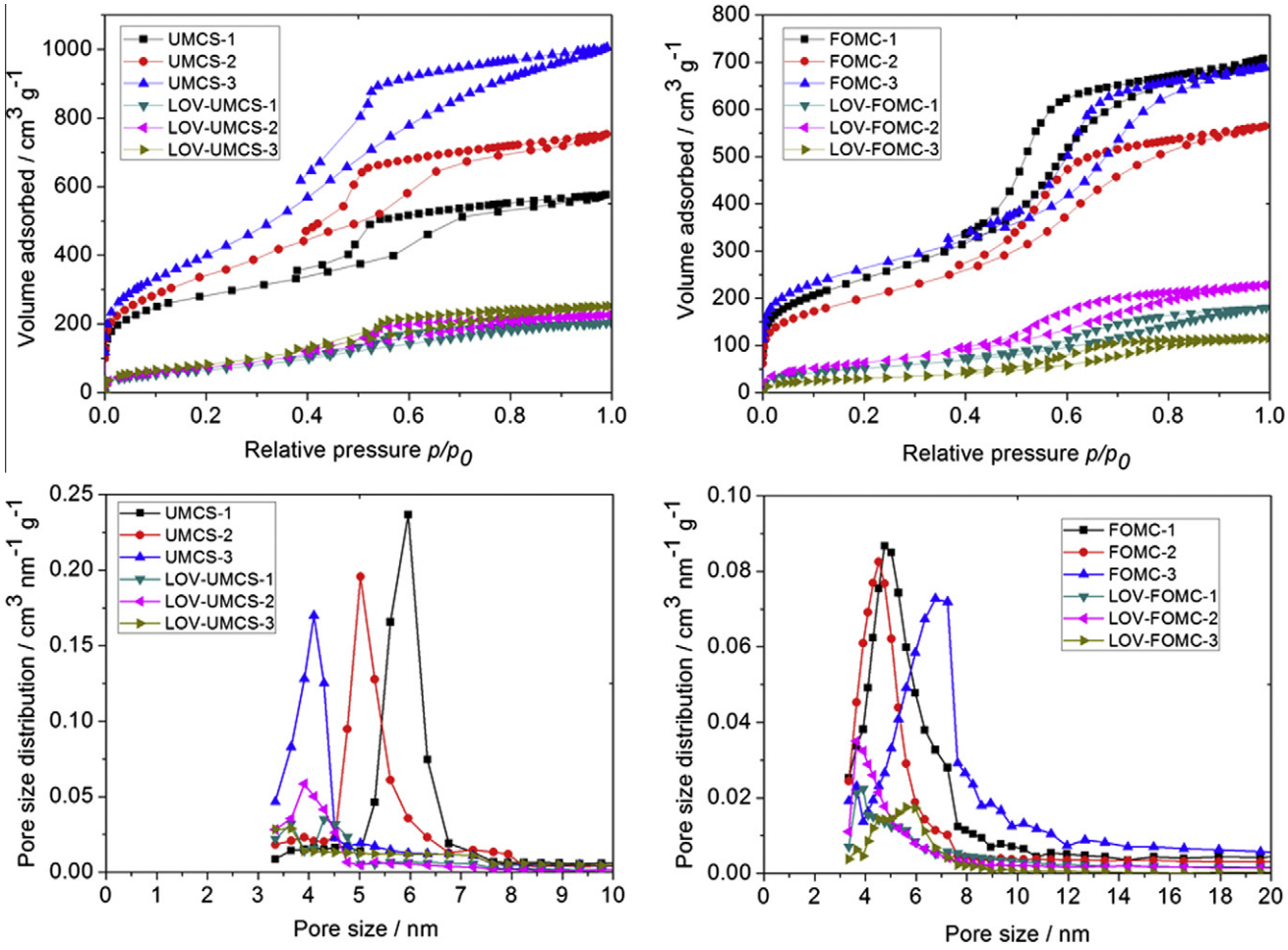

Fig. 5. Adsorption–desorption isotherms and pore size distribution. (For interpretation of the references to color in this figure legend, the reader is referred to the web version of this article.)

Table 1
Nanoparticle characterization and degree of drug loading of the samples.

Sample	Surface area ($m^2\ g^{-1}$)	Pore volume ($cm^3\ g^{-1}$)	Pore size (nm)	Degree of drug loading (%)
UMCS-1	1069	1.49	6.0	
UMCS-2	1246	1.26	5.1	
UMCS-3	1457	1.02	3.8	
FOMC-1	870	1.09	5.0	
FOMC-2	722	0.87	4.4	
FOMC-3	938	1.06	7.0	
LOV–UMCS-1	244	0.3122	4.3	28.66
LOV–UMCS-2	272	0.3483	3.9	31.21
LOV–UMCS-3	303	0.3885	3.6	36.26
LOV–FOMC-1	189	0.2758	3.9	27.85
LOV–FOMC-2	235	0.3510	3.7	25.63
LOV–FOMC-3	110	0.1770	5.6	30.17

compounds, the solubility of the noncrystalline form is usually higher than that of the crystalline form due to the relatively weaker binding energy. So, this may result in the enhanced solubility of LOV loaded into the carriers and further improve the dissolution rate of LOV from drug-loaded samples. The disappearance of characteristic LOV peaks in LOV–UMCS and LOV–FOMC may be due to following process. Firstly, LOV was present in a crystalline state, and after dissolving in methanol, it changed into a molecular form; subsequently, LOV was absorbed into the pore channels of UMCS and FOMC in molecular form during the drug loading process. Then, methanol was removed at 30 °C, and LOV was present in a noncrystalline form both inside and outside the carriers.

3.5. DSC analysis

We know that a pure crystalline drug can exhibit a depression of its melting point in the DSC curve. However, no depression can be detected if the compound is present in a noncrystalline state [42]. The DSC curves of pure crystalline LOV, the physical mixture, the drug-loaded samples, and carriers are shown in Fig. 7. For pure crystalline LOV, the melting point was 171.9 °C and a single peak at this temperature was clearly seen in its DSC curve, and there was no depression in the curves of UMCS and FOMC. However, for the drug-loaded samples LOV–UMCS and LOV–FOMC, the strength of this characteristic peak fell sharply and even disappeared, illustrating that the crystalline form of LOV had changed into a noncrystalline form during the drug loading process. This also supports the results of the WAXS study. This could also result in an enhanced dissolution rate and improved oral bioavailability.

3.6. XPS studies

XPS was used to determine the chemical composition present in the surface layer (about 10–15 nm in depth) of carriers and drug-loaded samples [43]. The atomic ratios were calculated according to the photoelectron peak area and used sensitivity

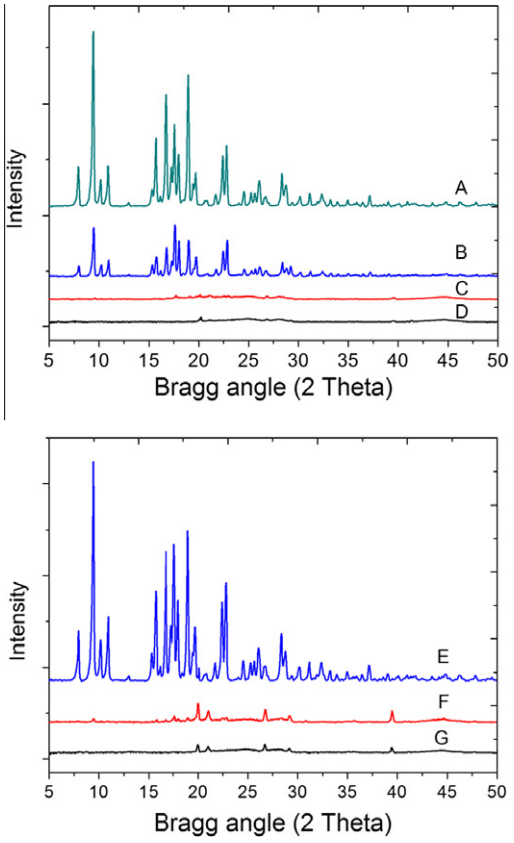

Fig. 6. WAXS patterns of (A) pure crystalline LOV, (B) physical mixture for UMCS and LOV, (C) LOV–UMCS, (D) UMCS, (E) physical mixture for FOMC and LOV, (F) LOV–FOMC, and (G) FOMC. (For interpretation of the references to color in this figure legend, the reader is referred to the web version of this article.)

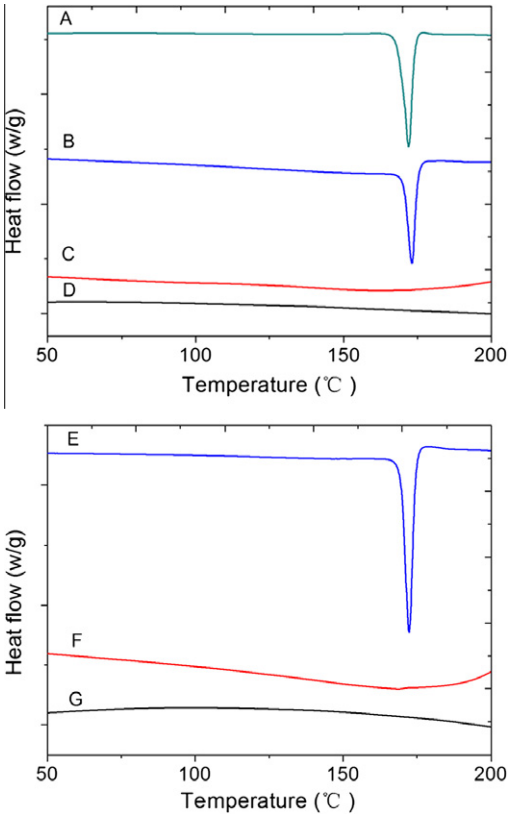

Fig. 7. DSC thermograms of (A) pure crystalline LOV, (B) physical mixture of UMCS and LOV, (C) LOV–UMCS, (D) UMCS, (E) physical mixture for FOMC and LOV, (F) LOV–FOMC, and (G) FOMC. (For interpretation of the references to color in this figure legend, the reader is referred to the web version of this article.)

factors according to the transmission features of the Physical Electronics SCA. The XPS spectra of LOV–UMCS and LOV–FOMC are presented in Fig. 8, and the ratio between carbon, oxygen, and degree of drug loading in the surface layer is given in Table 2. LOV loaded on the surface of carriers can also be calculated from the ratio of the composition. Both UMCS and FOMC are carbon and do not contain oxygen, while the model drug LOV ($C_{24}H_{36}O_5$) contains oxygen and, so, oxygen was chosen as the model element to account for the ratio of drug in the surface layer of the samples. The presence of oxygen in the drug-loaded samples also proves that LOV was loaded into UMCS and FOMC. According to the results obtained, the ratio of drug on the surface of the samples analyzed by XPS was slightly higher than the full degree of drug loading determined by UV, suggesting that LOV is present both inside and outside the carriers in the drug-loaded samples. This also demonstrates the potential of UMCS and FOMC for use as vehicles in drug delivery systems.

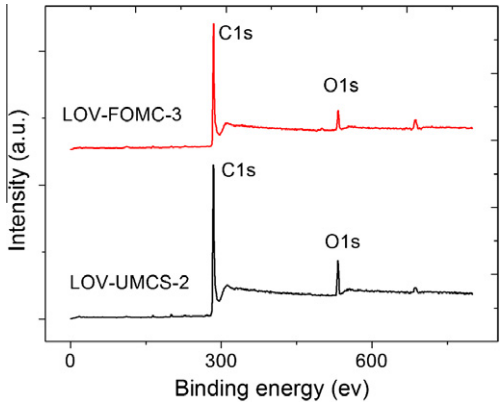

Fig. 8. XPS scan spectra of drug-loaded samples. (For interpretation of the references to color in this figure legend, the reader is referred to the web version of this article.)

3.7. In vitro release profiles

Fig. 9 shows the dissolution release profile of pure crystalline LOV and LOV from drug-loaded samples. LOV, which belongs to Biopharmaceutical Classification System II, has a very poor solubility in water and the gastrointestinal tract, resulting in a very slow release rate. Also, the cumulative dissolution of pure crystalline LOV in the dissolution medium was only about 30% after 90 min, which results in a poor absorption and low oral bioavailability (20–40%). For the drug-loaded samples LOV–FOMC, a much faster dissolution rate was seen compared with that of pure crystalline LOV. The cumulative dissolution of LOV in buffer (pH 6.8) was more than 55% at the sampling time of 10 min for LOV–FOMC. The increased dissolution may be due to the following factors: (1)

Table 2
The composition and degree of drug loading on the surface.

Samples	C (%)	O (%)	Degree of drug loading on the surface (%)
LOV–UMCS-2	91.55	8.45	52.77
LOV–FOMC-3	93.98	6.02	38.41

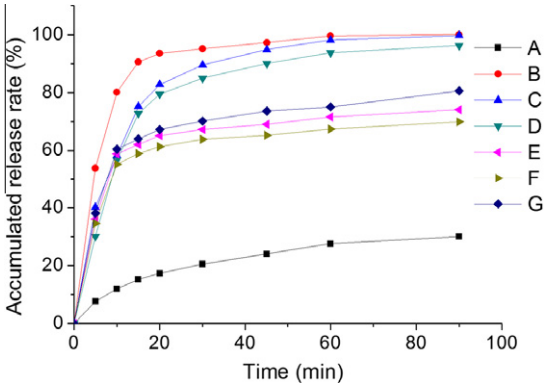

Fig. 9. Release profiles of LOV from (A) pure crystalline LOV, (B) LOV–UMCS-1, (C) LOV–UMCS-2, (D) LOV–UMCS-3, (E) LOV–FOMC-1, (F) LOV–FOMC-2, and (G) LOV–FOMC-3. (For interpretation of the references to color in this figure legend, the reader is referred to the web version of this article.)

The change in LOV from the crystalline state to the noncrystalline state results in increased solubility and reduced binding energy; (2) the high dispersibility of the drug in the pore channels of the carriers; (3) in drug-loaded samples, the particle size of the drug is reduced significantly, which can markedly increase the surface area and contact between the drug and dissolution medium; (4) carbon is an inert substance and has no functional groups on its surface, so the force is physical adsorption (Van der Waals adsorption) during the drug loading procedure. For physical adsorption, the bonding force is much weaker, and the energy of adsorption is much smaller than in the case of chemical adsorption. So, the adsorption rate and desorption rates are both fast, and in addition, this adsorption is reversible, so water molecules can easily disrupt the adsorptive power between drug and carriers. All of these factors result in a fast release of drug in the dissolution medium. In addition, LOV–FOMC-3 exhibits the fastest dissolution rate among the drug-loaded samples using FOMC as carriers, and this may due to its relatively larger pore size (7.0 nm). However, after 15 min, the dissolution rate becomes slower compared with that during the initial 15 min, and the cumulative dissolution was only 70–80% at the sampling time of 90 min. The reason for this is that part of the LOV was absorbed on the surface layer of the carrier and the remainder was loaded into the internal pore channels, so the drug in the surface layer release rapidly in the dissolution medium, so-called burst release, while the drug inside the FOMC had to pass through the porous channel before dispersing in the medium. The length of the FOMC channels is longer than that of UMCS, so this part of the drug exhibits a relatively sustained-release profile compared with CEL-UMCS.

For LOV–UMCS, the dissolution profile of LOV exhibited a faster dissolution rate than that of LOV–FOMC, and the cumulative dissolution of LOV from LOV–UMCS was 70–90% at the sampling time of 15 min; this rose to 90% at the sampling time of 45 min. In addition, UMCS has a continuous 3-D pore system, and the length of pore channels is much shorter (less than 400 nm) compared with FOMC. This is why it exhibits a faster release rate compared with FOMC as drug delivery vehicle. LOV–UMCS-1 has the fastest release rate compared with LOV–UMCS-2 and LOV–UMCS-3 due to its relatively larger pore diameter (6.0 nm). Accordingly, the larger the mesopores are, the faster the dissolution rate is. This may be due to the fact that large pores can reduce the resistance when a drug passes through the pore channels.

All of these findings support the advantages of mesoporous carbon with different pore sizes and structures as an important drug delivery vehicle for controlled release of poorly water soluble drugs.

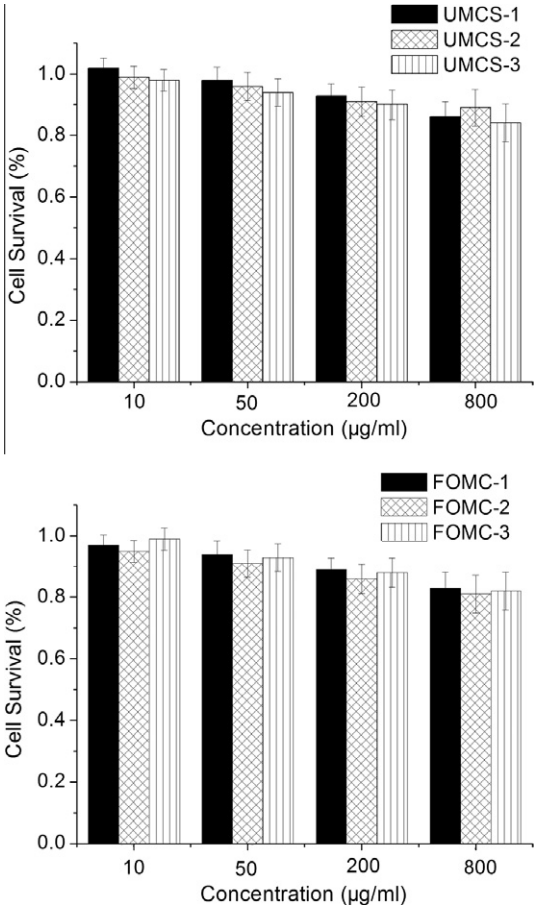

Fig. 10. Cytotoxicity study of UMCS and FOMC on Caco-2 cells.

3.8. Cytotoxicity assays

Fig. 10 shows the survival rate of Caco-2 cells after a 24 h exposure to carriers. Both UMCS and FOMC exhibit no apparent cytotoxicity to Caco-2 cells at the tested concentrations (10–800 μg/ml). When the concentration of carriers increased, cell survival was slightly reduced, and this weak toxic effect observed at high concentrations might be attributed to carrier agglomeration [44] in aqueous culture medium, as a result of strong Van der Waal's interactions [45]. However, even at a concentration of 800 μg/ml, the cell survival remained above 80%, confirming the weak cytotoxicity of the mesoporous carbon matrix. Images of Caco-2 cells (Fig. 11) showed that the growth of Caco-2 cells following the addition of UMCS and FOMC was unchanged compared with that of normal Caco-2 cells. All were able to adhere to the bottom of culture flasks and maintain a fast growth rate, demonstrating the safety of UMCS and FOMC when used as drug delivery vehicles.

4. Conclusion

UMCS and FOMC were successfully synthesized, and their pharmaceutical performance as a carrier was investigated first time. They were all found to possess high surface area, large pore volume, and uniform pore diameter. UMCS and FOMC exhibited a high degree of drug loading. In the in vitro release study, both LOV–UMCS and LOV–FOMC exhibited a much faster dissolution rate compared with pure crystalline drug. In addition, differences in pore diameter also have an influence on controlling the release of poorly water soluble drugs, and carriers with a larger pore size produce a faster dissolution rate. The porous structure of carriers also has an effect on release of drug from drug-loaded samples.

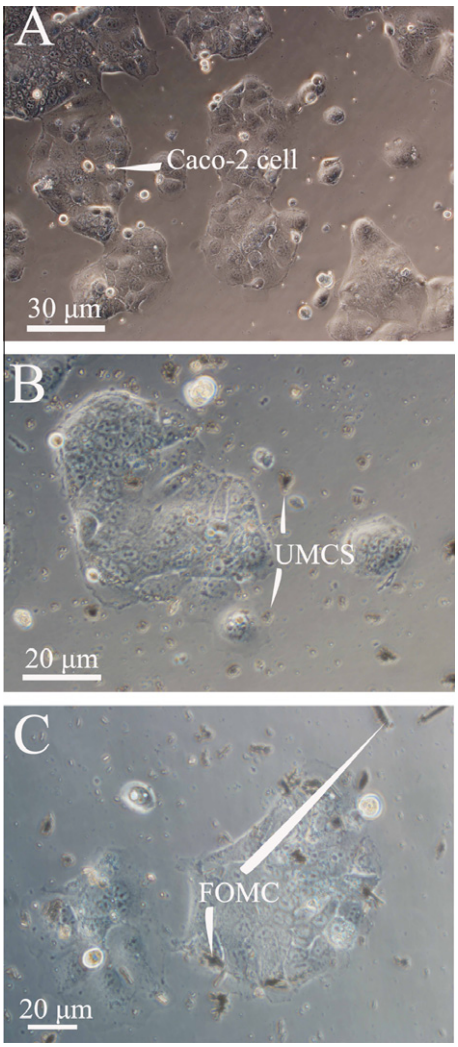

Fig. 11. Morphology of (A) Caco-2 cells, (B) Caco-2 cells added UMCS, and (C) Caco-2 cells added FOMC. (For interpretation of the references to color in this figure legend, the reader is referred to the web version of this article.)

UMCS with a 3-D pore system is better in improving the dissolution rate of insoluble drugs compared with FOMC which has a 2-dimensional hexagonal mesoporous structure. In addition, both UMCS and FOMC exhibited low toxicity in cytotoxicity assays, confirming the safety of mesoporous carbon when used as a drug delivery carrier. These factors all support the potential and advantages of using mesoporous carbon as a carrier in drug delivery systems. We believe this research is a significant contribution to the design of oral drug delivery systems and the controlled release of poorly water soluble drugs.

Acknowledgements

This work was supported by the National Basic Research Program of China (973 Program) (No. 2009CB930300) and Major National Platform for Innovative Pharmaceuticals (No. 2009ZX09301-012). We would like to thank Dr. David Jack for correcting language.

References

[1] Y.H. Liu, C.S. Sun, Y.R. Hao, T.Y. Jiang, L. Zheng, S.L. Wang, Mechanism of dissolution enhancement and bioavailability of poorly water soluble celecoxib by preparing stable amorphous nanoparticles, J. Pharm. Pharm. Sci. 13 (2010) 589–606.
[2] A.S. Al-Kady, M. Gaber, M.M. Hussein, E.M. Ebeid, Nanostructure-loaded mesoporous silica for controlled release of coumarin derivatives: a novel testing of the hyperthermia effect, Eur. J. Pharm. Biopharm. 77 (2011) 66–74.
[3] S. Polarz, B. Smarsly, H. Schattka, Hierachical porous carbon structures from cellulose acetate fibers, Chem. Mater. 14 (2002) 2940–2945.
[4] R. Mellaerts, R. Mols, J.A.G. Jammaer, C.A. Aerts, P. Annaert, J.V. Humbeeck, G.V.D. Mooter, P. Augustijns, J.A. Martens, Increasing the oral bioavailability of the poorly water soluble drug itraconazole with ordered mesoporous silica, Eur. J. Pharm. Biopharm. 69 (2008) 223–230.
[5] P. Valle-Vigón, M. Sevilla, A.B. Fuertes, Synthesis of uniform mesoporous carbon capsules by carbonization of organosilica nanospheres, Chem. Mater. 22 (2010) 2526–2533.
[6] D.J. Bindl, M.Y. Wu, F.C. Prehn, M.S. Arnold, Efficiently harvesting excitons from electronic type-controlled semiconducting carbon nanotube films, Nano Lett. 11 (2011) 455–460.
[7] M.V. Speybroeck, R. Mols, R. Mellaerts, T.D. Thi, J.A. Martens, J.V. Humbeeck, P. Annaert, G.V.D. Mooter, P. Augustijns, Combined use of ordered mesoporous silica and precipitation inhibitors for improved oral absorption of the poorly soluble weak base itraconazole, Eur. J. Pharm. Biopharm. 75 (2010) 354–365.
[8] Y.Z. Zhang, Z.Z. Zhi, T.Y. Jiang, J.H. Zhang, Z.Y. Wang, S.L. Wang, Spherical mesoporous silica nanoparticles for loading and release of the poorly water-soluble drug telmisartan, J. Control. Release 145 (2010) 257–263.
[9] Y.Z. Zhang, J.H. Zhang, T.Y. Jiang, S.L. Wang, Inclusion of the poorly water-soluble drug simvastatin in mesocellular foam nanoparticles: drug loading and release properties, Int. J. Pharm. 410 (2011) 118–124.
[10] T. Heikkilä, H.A. Santos, N. Kumar, D.Y. Murzin, J. Salonen, T. Laaksonen, L. Peltonen, J. Hirvonen, V.-P. Lehto, Cytotoxicity study of ordered mesoporous silica MCM-41 and SBA-15 microparticles on Caco-2 cells, Eur. J. Pharm. Biopharm. 74 (2010) 483–494.
[11] F.Q. Zhang, D. Gu, T. Yu, F. Zhang, S.H. Xie, L.J. Zhang, Y.H. Deng, Y. Wan, B. To, D.Y. Zhao, Mesoporous carbon single-crystals from organic–organic self-assembly, J. Am. Chem. Soc. 129 (2007) 7746–7747.
[12] C. Charnay, S. Bégu, C. Tourné-Péteilh, L. Nicole, D.A. Lerner, J.M. Devoisselle, Inclusion of ibuprofen in mesoporous templated silica: drug loading and release property, Eur. J. Pharm. Biopharm. 57 (2004) 533–540.
[13] M. Yu, H.H. Funke, J.L. Falconer, R.D. Noble, High Density, Vertically-aligned carbon nanotube membranes, Nano Lett. 9 (2009) 225–229.
[14] L.C. Yin, R. Saito, M.S. Dresselhaus, The fermi level dependent electronic properties of the smallest (2,2) carbon nanotube, Nano Lett. 10 (2010) 3290–3296.
[15] C. Wu, Z.Y. Wang, Z.Z. Zhi, T.Y. Jiang, J.H. Zhang, S.L. Wang, Development of biodegradable porous starch foam for improving oral delivery of poorly water soluble drugs, Int. J. Pharm. 403 (2011) 162–169.
[16] Y.Z. Zhang, T.Y. Jiang, Q. Zhang, S.L. Wang, Inclusion of telmisartan in mesocellular foam nanoparticles: drug loading and release property, Eur. J. Pharm. Biopharm. 76 (2010) 17–23.
[17] D. Carriazo, M.C. Gutiérrez, M.L. Ferrer, F.D. Monte, Resorcinol-based deep eutectic solvents as both carbonaceous precursors and templating agents in the synthesis of hierarchical porous carbon monoliths, Chem. Mater. 22 (2010) 6146–6152.
[18] S. Zhao, C.Y. Wang, M.M. Chen, Z.Q. Shi, Preparation of carbon sphere from corn starch by a simple method, Mater. Lett. 62 (2008) 3322–3324.
[19] X.Y. Wang, H.Q. Wang, Q.F. Dai, Q.Y. Li, J.H. Yang, A.N. Zhang, Z.X. Yan, Preparation of novel porous carbon spheres from corn starch, Colloids Surf. A 346 (2009) 213–215.
[20] H.Q. Wang, Q.F. Dai, Q.Y. Li, J.H. Yang, X.X. Zhong, Y.G. Huang, A.N. Zhang, Z.X. Yan, Preparation of porous carbon spheres from porous starch, Solid State Ionics 180 (2009) 1429–1432.
[21] N. Gokulakrishnan, N. Kania, B. Léger, C. Lancelot, D. Grosso, E. Monflier, A. Ponchel, An ordered hydrophobic P6mm mesoporous carbon with graphitic pore walls and its application in aqueous catalysis, Carbon 49 (2011) 1290–1298.
[22] G.L. Cui, L.J. Zhi, A. Thomas, U. Kolb, I. Lieberwirth, K. M-llen, One-dimensional porous carbon/platinum composites for nanoscale electrodes, Angew. Chem. Int. Ed. 46 (2007) 3464–3467.
[23] C.W. Huang, C.H. Hsu, P.L. Kuo, C.T. Hsieh, H. Teng, Mesoporous carbon spheres grafted with carbon nanofibers for high-rate electric double layer capacitors, Carbon 49 (2011) 895–903.
[24] S.H. Joo, S.J. Choi, I. Oh, J. Kwak, Z. Liu, O. Terasaki, R. Ryoo, Ordered nanoporous arrays of carbon supporting high dispersions of platinum nanoparticles, Nature 412 (2001) 169–172.
[25] Z.L. Schaefer, M.L. Gross, M.A. Hickner, R.E. Schaak, Uniform hollow carbon shells: nanostructured graphitic supports for improved oxygen-reduction catalysis, Angew. Chem. Int. Ed. 49 (2010) 7045–7048.
[26] C. Vix-Guterl, E. Frackowiak, K. Jurewicz, M. Friebe, J. Parmentier, F. Béguin, Electrochemical energy storage in ordered porous carbon materials, Carbon 43 (2005) 1293–1302.
[27] L.W. Ji, Z. Lin, A.J. Medford, X.W. Zhang, Porous carbon nanofibers from electrospun polyacrylonitrile/SiO_2 composites as an energy storage material, Carbon 47 (2009) 3346–3354.
[28] D. Banham, F.X. Feng, J. Burt, E. Alsrayheen, V. Birss, Bimodal, templated mesoporous carbons for capacitor applications, Carbon 48 (2010) 1056–1063.
[29] A.O. Fung, C. Tsiokos, O. Paydar, L.H. Chen, S. Jin, Y.B. Wang, J.W. Judy, Electrochemical properties and myocyte interaction of carbon nanotube microelectrodes, Nano Lett. 10 (2010) 4321–4327.

[30] S.M. Cooper, B.A. Cruden, M. Meyyappan, Gas transport characteristics through a carbon nanotubule, Nano Lett. 4 (2004) 377–381.
[31] X. Xie, L.B. Hu, M. Pasta, G.F. Wells, D.S. Kong, C.S. Criddle, Y. Cui, Three-dimensional carbon nanotube–textile anode for high-performance microbial fuel cells, Nano Lett. 11 (2011) 291–296.
[32] L. Radhakrishnan, J. Reboul, S.H. Furukawa, P. Srinivasu, S. Kitagawa, Y. Yamauchi, Preparation of microporous carbon fibers through carbonization of Al-based porous coordination polymer (Al-PCP) with furfuryl alcohol, Chem. Mater. 23 (2011) 1225–1231.
[33] J.Y. Kim, S.B. Yoon, J.S. Yu, Template synthesis of a new mesostructured silica from highly ordered mesoporous carbon molecular sieves, Chem. Mater. 15 (2003) 1932–1934.
[34] K. Xia, Q.M. Gao, C.D. Wu, S.Q. Song, M.L. Ruan, Activation, characterization and hydrogen storage properties of the mesoporous carbon CMK-3, Carbon 45 (2007) 1989–1996.
[35] Z.J. Li, W.F. Yan, S. Dai, A novel vesicular carbon synthesized using amphiphilic carbonaceous material and micelle templating approach, Carbon 42 (2004) 767–770.
[36] J. Lee, J. Kim, T. Hyeon, Recent progress in the synthesis of porous carbon materials, Adv. Mater. 18 (2006) 2073–2094.
[37] P. Göring, E. Pippel, H. Hofmeister, R.B. Wehrspohn, M. Steinhart, L. Gösele, Gold/carbon composite tubes and gold nanowires by impregnating templates with hydrogen tetrachloroaurate/acetone solutions, Nano Lett. 4 (2004) 1121–1125.
[38] S.M. Zhua, C.X. Chen, Z.X. Chen, X.Y. Liu, Y. Li, Y. Shi, D. Zhang, Thermo-responsive polymer-functionalized mesoporous carbon for controlled drug release, Mater. Chem. Phys. 126 (2010) 357–363.
[39] X.F. Wang, P. Liu, Y. Tian, Ordered mesoporous carbons for ibuprofen drug loading and release behavior, Micropor. Mesopor. Mater. 142 (2011) 334–340.
[40] S.M. Taghdisi, P. Lavaee, M. Ramezani, K. Abnous, Reversible targeting and controlled release delivery of daunorubicin to cancer cells by aptamer-wrapped carbon nanotubes, Eur. J. Pharm. Biopharm. 77 (2011) 200–206.
[41] D.Y. Zhao, J.L. Feng, Q.S. Huo, N. Melosh, G.H. Fredrickson, B.F. Chmelka, G.D. Stucky, Triblock copolymer syntheses of mesoporous silica with periodic 50 to 300 angstrom pores, Science 279 (1998) 548–552.
[42] J. Salonen, L. Laitinen, A.M. Kaukonen, J. Tuura, M. Björkqvist, T. Heikkilä, K. Vähä-Heikkilä, J. Hirvonen, V.P. Lehto, Mesoporous silicon microparticles for oral drug delivery: Loading and release of five model drugs, J. Control. Release 108 (2005) 362–374.
[43] J.L. Figueiredo, M.F.R. Pereira, M.M.A. Freitas, J.J.M. Órfão, Modification of the surface chemistry of activated carbons, Carbon 37 (1999) 1379–1389.
[44] P. Wick, P. Manser, L.K. Limbach, U. Dettlaff-Weglikowska, F. Krumeich, S. Roth, W.J. Stark, A. Bruinink, The degree and kind of agglomeration affect carbon nanotube cytotoxicity, Toxicol. Lett. 168 (2007) 121–131.
[45] L. Zhang, L. Zeng, A.R. Barron, N.A. Monteiro-Riviere, Biological interactions of functionalized single-wall carbon nanotubes in human epidermal keratinocytes, Int. J. Toxicol. 26 (2007) 103–113.